Progress In Electromagnetics Research C, Vol. 53, 55–66, 2014

Design of Compact Wideband High-Selectivity Band-Stop Filter Based on Coupled Lines

Menglou Rao, Yongle Wu*, Weimin Wang, and Yuanan Liu

Abstract—In this paper, a compact band-stop filter with a wideband and high-selectivity performance is proposed and analyzed. This band-stop filter includes two parallel-coupled lines of different electrical lengths and two open-circuit stubs. A lossless transmission line model is used to obtain the filter design parameters. In order to verify this new filter circuit structure and its corresponding design theory, five groups of numerical examples are demonstrated. Finally, a practical band-stop filter with a 3-dB cutoff frequency bandwidth of 58.2% centered at 0.94 GHz has been designed, simulated and measured. The measured results show a good agreement with the simulated responses.

1. INTRODUCTION

Wideband band-stop filters are in increasing demand in microwave circuit applications to suppress undesired wideband signals. The conventional microstrip band-stop filter [1] has open-circuited stubs and shunt stubs of a quarter-wavelength. However, the bandwidth of this filter is narrow and the upper band-stop center frequency is located at three times of the operating center frequency in the fundamental stopband. To meet the requirement of low insertion loss and sharp rejection, various structures and bandwidth enhancement technologies for band-stop filters have been developed in recent years [2–9]. For example, a compact band-stop filter using Defected Microstrip Structure (DMS) by etching Open Square Ring (OSR) is proposed in [2], which has low insertion loss in the passband and high rejection level. The T-shaped defected microstrip structures and the U-shaped defected ground structures are provided to create a novel miniaturized dual-band band-stop filter in [3]. Meanwhile, modified stubs are also applied to construct wideband band-stop filters in [4]. Coupled lines have been widely used for implementing filters for a long time. It can improve the upper pass-band performance in band-stop filters [5] and sharpen skirt selectivity of filters [6]. A compact microstrip coupled-line configuration has been presented to design an ultra-wideband band-stop filter in [7]. The band-stop filter presented in [8] also uses two symmetrical coupled-line stubs to form two shorted points to realize dual-stopband characteristics, which can work with low insertion loss in the passband and sharp rejection in the stopbands. In [9], a microstrip band-stop filter using two meandered parallel-coupled lines of different electrical lengths and characteristic impedances in shunt is presented. Yet, note that this band-stop filter has two obvious disadvantages: low selectivity and poor return loss in passband.

In order to remove these two limitations, a modified filter is discussed and proposed in this paper. Extended from the band-stop filter in [9], two open-circuit stubs are added symmetrically, thus this proposed structure is symmetrical. This improved circuit configuration has a higher selectivity, better return loss and lower insertion loss for passband. The total external performances can be expressed by closed-form mathematical expressions. The performance of this band-stop filter can be controlled by different even- and odd-mode characteristic impedances of the coupled lines and the characteristic impedances of the open-circuit stubs. To illustrate the effects of different kinds of impedance values, five parts of discussion are represented. According to the analysis, two types of ideal band-stop filters

Received 18 July 2014, Accepted 10 August 2014, Scheduled 23 August 2014
* Corresponding author: Yongle Wu (wuyongle138@gmail.com).
The authors are with School of Electronic Engineering, Beijing University of Posts and Telecommunications, Beijing, China.

with normal operating frequency (1 GHz) are designed, calculated and discussed by using lossless transmission-line and coupled-line models. Afterwards, the band-stop filter operating at 1 GHz has been simulated with a full-wave simulation tool. To verify the theoretical prediction, the filter is fabricated by using common microstrip technology. The measured results show that the 10-dB fractional bandwidth is from 0.71 GHz to 1.16 GHz. The passband insertion loss is smaller than 1.57 dB in the range of 0 to 0.65 GHz and smaller than 1.15 dB in the range of 1.3 to 2.6 GHz.

2. THE CIRCUIT STRUCTURE AND THEORY OF THE PROPOSED BAND-STOP FILTER

The proposed circuit structure of the band-stop filter is shown in Figure 1. Two parallel-coupled lines of different electrical lengths, and two open-circuit stubs are added in shunt symmetrically. The characteristic impedances of the two coupled lines are denoted as Z_{e1}, Z_{o1}, Z_{e2}, Z_{o2}, and the characteristic impedance of the open-circuit stub is Z_3. For convenience, both the upper and lower coupled line structures are assumed to have the same even- and odd-mode electrical length ($\theta_{c1} = \theta_{e1} = \theta_{o1}$, $\theta_{c2} = \theta_{e2} = \theta_{o2}$), and the corresponding electrical lengths of the open-circuit stubs are both θ_3. Z_T is the port impedance. According to the symmetrical network analysis results [1, 9], the network analysis of Figure 1 will be simplified by analyzing the one-port networks shown in Figure 2. Based on the analysis theory [1, 5], the input impedances Z_{ine} and Z_{ino} shown in Figure 2 can be expressed by

$$Z_{ine} = \frac{Z_{ine1} \times \dfrac{Z_3}{j \tan \theta_3}}{Z_{ine1} + \dfrac{Z_3}{j \tan \theta_3}}, \tag{1a}$$

$$Z_{ino} = \frac{Z_{ino1} \times \dfrac{Z_3}{j \tan \theta_3}}{Z_{ino1} + \dfrac{Z_3}{j \tan \theta_3}}, \tag{1b}$$

in which

$$Z_{ine1} = \frac{\dfrac{Z_{e1}}{j \tan \theta_{c1}} \times \dfrac{Z_{e2}}{j \tan \theta_{c2}}}{\dfrac{Z_{e1}}{j \tan \theta_{c1}} + \dfrac{Z_{e2}}{j \tan \theta_{c2}}}, \tag{2a}$$

$$Z_{ino1} = \frac{jZ_{o1} \tan \theta_{c1} \times jZ_{o2} \tan \theta_{c2}}{jZ_{o1} \tan \theta_{c1} + jZ_{o2} \tan \theta_{c2}}. \tag{2b}$$

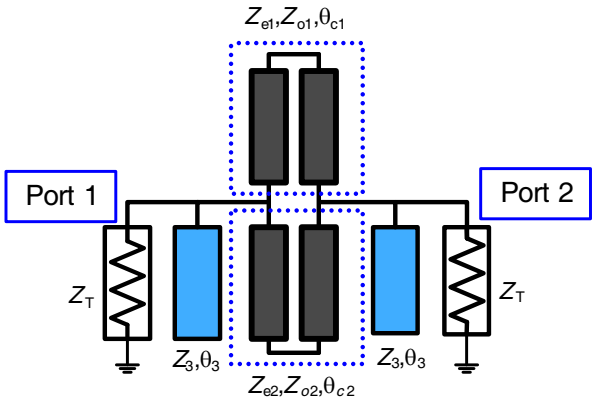

Figure 1. The circuit schematic of the proposed band-stop filter.

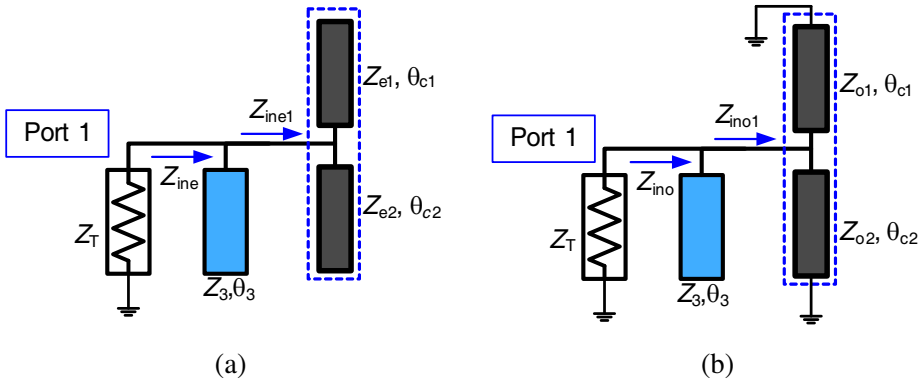

Figure 2. The equivalent simplified circuit structures of the band-stop filter under (a) even-mode and (b) odd-mode excitations.

Therefore, the even- and odd-mode input impedances Z_{ine} and Z_{ino} can be expressed as

$$Z_{ine} = -j\frac{Z_{e1}Z_{e2}Z_3}{Z_{e1}Z_{e2}\tan\theta_3 + Z_3(Z_{e1}\tan\theta_{c2} + Z_{e2}\tan\theta_{c1})}, \tag{3a}$$

$$Z_{ino} = j\frac{Z_{o1}Z_{o2}Z_3\tan\theta_{c1}\tan\theta_{c2}}{Z_3(Z_{o1}\tan\theta_{c1} + Z_{o2}\tan\theta_{c2}) - Z_{o1}Z_{o2}\tan\theta_{c1}\tan\theta_{c2}\tan\theta_3}. \tag{3b}$$

Then, the even- and odd-mode scattering parameters of this proposed band-stop filter can be calculated by [1]

$$S_{11e} = \frac{Z_{ine} - Z_T}{Z_{ine} + Z_T}, \tag{4a}$$

$$S_{11o} = \frac{Z_{ino} - Z_T}{Z_{ino} + Z_T}. \tag{4b}$$

When the symmetrical property is considered, the external scattering parameters can be expressed by [1]

$$S_{11} = S_{22} = \frac{S_{11e} + S_{11o}}{2}, \tag{5}$$

$$S_{21} = S_{12} = \frac{S_{11e} - S_{11o}}{2}. \tag{6}$$

By combining (4)–(6), the mathematical expressions of scattering parameters are

$$S_{11} = \frac{Z_{ine}Z_{ino} - Z_T^2}{(Z_{ine} + Z_T)(Z_{ino} + Z_T)}, \tag{7}$$

$$S_{21} = \frac{(Z_{ine} - Z_{ino})Z_T}{(Z_{ine} + Z_T)(Z_{ino} + Z_T)}. \tag{8}$$

The condition of transmission poles (reflection zeros) can be obtained when

$$|S_{11}| = 0, \tag{9}$$

and transmission zeros can be obtained when

$$|S_{21}| = 0. \tag{10}$$

Hence, the final Equations (9) and (10) including the characteristic impedances and electrical lengths are

$$\frac{Z_{e1}Z_{e2}Z_{o1}Z_{o2}Z_3^2\tan\theta_{c1}\tan\theta_{c2}}{\begin{array}{l}[Z_{e1}Z_{e2}\tan\theta_3 + Z_3(Z_{e1}\tan\theta_{c2} + Z_{e2}\tan\theta_{c1})] \\ \times[Z_3(Z_{o1}\tan\theta_{c1} + Z_{o2}\tan\theta_{c2}) - Z_{o1}Z_{o2}\tan\theta_{c1}\tan\theta_{c2}\tan\theta_3]\end{array}} = Z_T^2, \tag{11}$$

and

$$\frac{Z_{e1} \times Z_{e2}}{Z_{e1} \tan\theta_{c2} + Z_{e2} \tan\theta_{c1}} = j \frac{Z_{o1} Z_{o2} \tan\theta_{c1} \tan\theta_{c2}}{Z_{o1} \tan\theta_{c1} + Z_{o2} \tan\theta_{c2}}. \quad (12)$$

According to the analytical Equations (1)–(12), the external scattering parameters performance (including magnitude and phase information) of this novel band-stop filter can be calculated and analyzed. The band-stop filter's center frequency is normalized at 1 GHz, and it leads to transmission zeros distributed by pairs symmetrically placed around the center frequency. If the line lengths are chosen appropriately, the band-stop performance at the operating frequency will be determined.

3. ANALYSIS OF CIRCUIT ELECTRICAL PARAMETERS

To illustrate the performance of the filter, which is affected by characteristic impedances of the coupled lines (Z_{e1},Z_{o1},Z_{e2},Z_{o2}) and the open-circuit stubs (Z_3), five parts of discussion will be represented according to the proposed analytical approach above. For simplicity, the electrical lengths have been decided as $\theta_{c1} = \frac{3}{4}\pi$, $\theta_{c2} = \frac{\pi}{4}$, $\theta_3 = \frac{\pi}{2}$, and all values of the port impedance Z_T of the following examples are equal to$50\,\Omega$.

3.1. The influence of Z_{e2} and Z_{o2} on the Transmission Zeros and Reflection Zeros of the Proposed Filter

It can be observed from the Equations (11) and (12) that the transmission zero of the filter is determined by Z_{e1}, Z_{o1}, Z_{e2}, Z_{o2} as well as θ_{c1} and θ_{c2}. In the case that θ_{c1} and θ_{c2} are predetermined, the values of Z_{e1}, Z_{o1}, Z_{e2}, Z_{o2} are important factors leading to various transmission zeros and reflection zeros. The analysis of Z_{e2} and Z_{o2} is taken for example. The frequency points of transmission zeros and reflection zeros with different Z_{e2} and Z_{o2} are plotted in Figure 3 and Figure 4 respectively. The rest of the design parameters are uniformly determined as $Z_{e1} = 140\,\Omega$, $Z_{o1} = 105\,\Omega$, $Z_3 = 122\,\Omega$. It can be clearly observed in Figure 3 and Figure 4 that the number of transmission zeros is affected by Z_{e2} and Z_{o2}. In Figure 3, Z_{o2} is fixed as $120\,\Omega$. When $Z_{e2} < 115\,\Omega$, the filter has three transmission zeros in the stopband. The number of zeros decreases to two when $115\,\Omega < Z_{e2} < 123\,\Omega$. And when $Z_{e2} > 123\,\Omega$, there is just one zero in the stopband. In Figure 4, Z_{e2} is fixed as $140\,\Omega$. Similarly, the filter has three transmission zeros when $Z_{o2} < 103\,\Omega$, two zeros when $103\,\Omega < Z_{o2} < 109\,\Omega$ and one when $Z_{o2} > 109\,\Omega$. Besides, Figure 3 shows that the upper reflection zero becomes closer to the transmission zero when Z_{e2} increases while the lower has no obvious change. The lower reflection zero increases when Z_{o2} increases while the upper invariants in Figure 4. In other words, the selectivity is optimized with the increase of

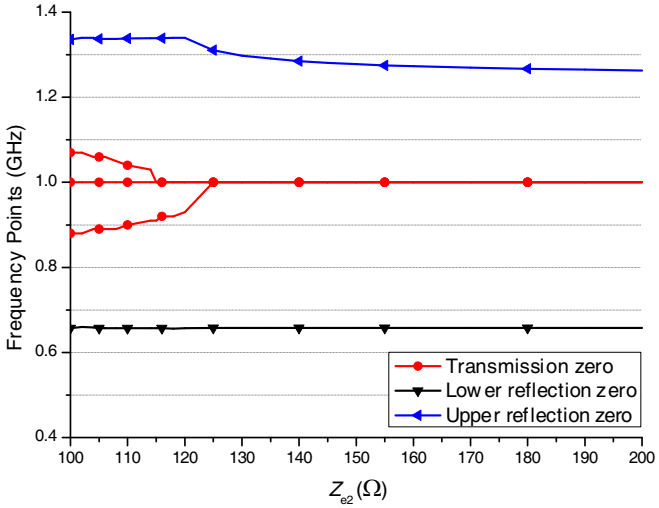

Figure 3. Frequencies of transmission zeros and reflection zeros with different Z_{e2}.

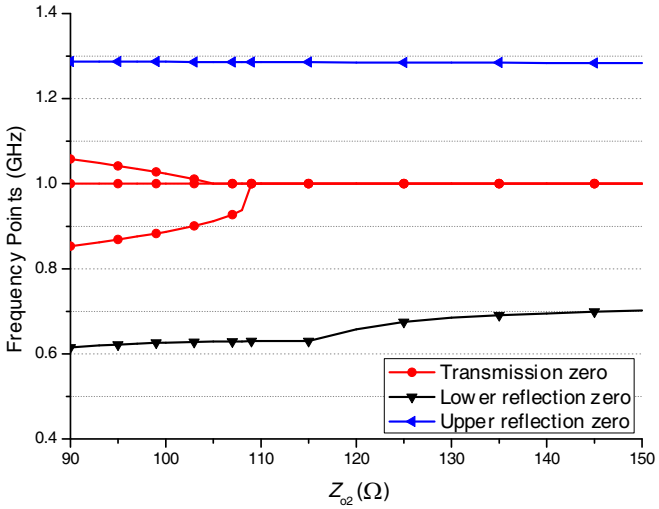

Figure 4. Frequencies of transmission zeros and reflection zeros with different Z_{o2}.

Z_{e2} and Z_{o2}. Figure 3 and Figure 4 can be considered as a useful guidance of the selection of Z_{e2} and Z_{o2}.

3.2. The Influence of Z_{e1} on the Performance of the Proposed Filter

When other electrical parameters are fixed, the variation of Z_{o1} and Z_{e1} will affect the characteristics of the filter. For convenience, only the value of Z_{e1} has been changed. The electrical parameters' values of the filter are given in Table 1. Based on these values, the ideal scattering parameters can be calculated using Equations (1)–(12), and their magnitude responses are plotted in Figures 5(a) and (b) respectively. From Figure 5(a), it can be seen that the return loss in passband changes regularly with the variation of Z_{e1}: Example A_4 has the highest passband return loss (larger than 23 dB) while Example A_1 has the lowest one (smaller than 17 dB). Furthermore, the first reflection zero decreases with Z_{e1} increasing. And the number of reflection zeros is six in Example A_1 while the number of the other three examples is seven. Therefore different numbers of reflection zeros can be obtained by choosing Z_{e1} properly. Besides, the selectivity is improved when Z_{e1} increases, as illustrated in Figure 5(b).

Table 1. The electrical parameters' values for the band-stop filter with variable Z_{e1}.

Parameters	Example A_1	Example A_2	Example A_3	Example A_4
Z_{e1} (Ω)	110	125	140	155
Z_{o1} (Ω)	105	105	105	105
Z_{e2} (Ω)	140	140	140	140
Z_{o2} (Ω)	120	120	120	120
Z_3 (Ω)	122	122	122	122

3.3. The Influence of Z_{e2} on the Performance of the Proposed Filter

Similar to the analytical approach in Section 3.2, only the value of Z_{e2} is changed while the other electrical parameters are determined. The circuit parameters' values are listed in Table 2 and the corresponding scattering parameters are plotted in Figures 6(a) and (b). It can be observed in Figure 6 that the value of Z_{e2} obviously affects the upper passband performance. Separation of reflection zeros in upper passband decreases with the increasing Z_{e2}, and the maximum return loss increases at the same time. In addition, the selectivity decreases with Z_{e2} increasing.

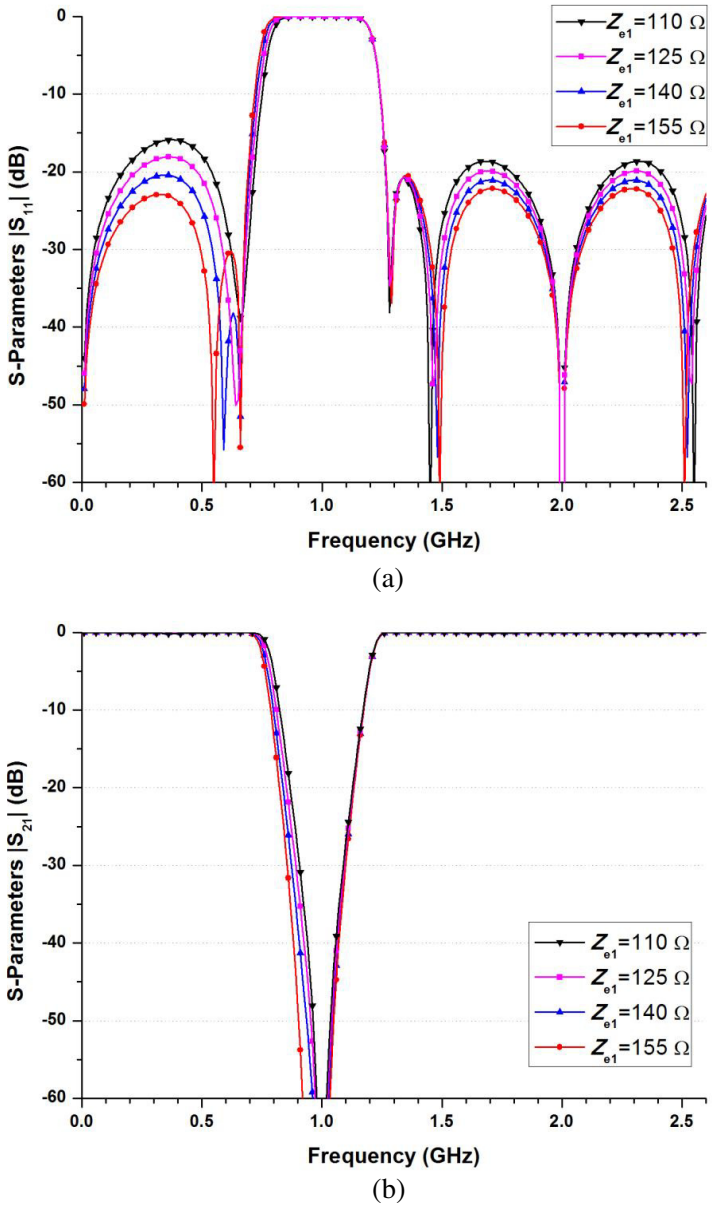

Figure 5. The scattering parameters (a) $|S_{11}|$ and (b) $|S_{21}|$ of the bandstop filter when $Z_{e1} = 110$, 125, 140 and 155 Ω.

Table 2. The electrical parameters' values for the band-stop filter with variable Z_{e2}.

Parameters	Example B_1	Example B_2	Example B_3	Example B_4
Z_{e1} (Ω)	140	140	140	140
Z_{o1} (Ω)	105	105	105	105
Z_{e2} (Ω)	125	140	170	185
Z_{o2} (Ω)	120	120	120	120
Z_3 (Ω)	122	122	122	122

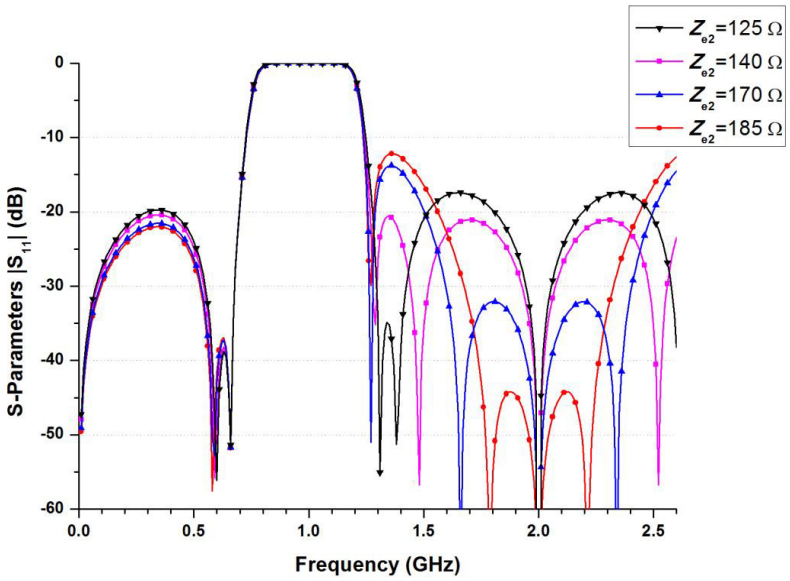

(a)

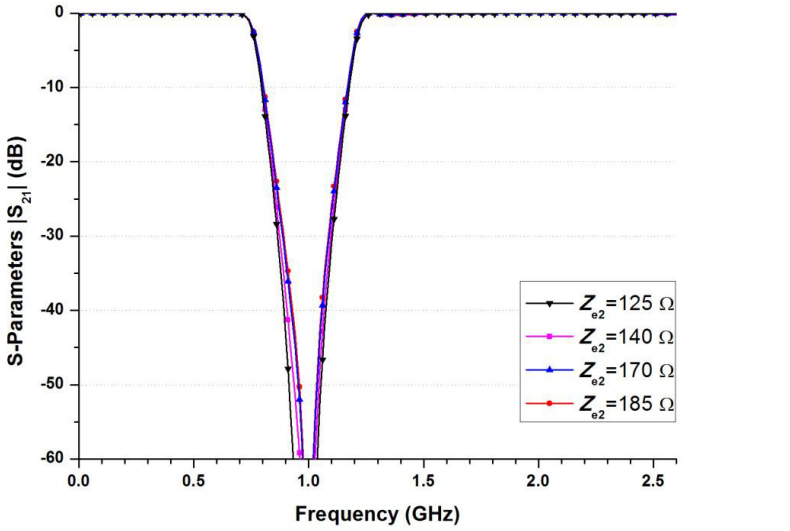

(b)

Figure 6. The scattering parameters (a) $|S_{11}|$ and (b) $|S_{21}|$ of the filter when Z_{e2} = 125, 140, 170, 185 Ω.

Table 3. The electrical parameters' values for the band-stop filter with variable Z_3.

Parameters	Example C_1	Example C_2	Example C_3	Example C_4
Z_{e1} (Ω)	140	140	140	140
Z_{o1} (Ω)	105	105	105	105
Z_{e2} (Ω)	140	140	140	140
Z_{o2} (Ω)	120	120	120	120
Z_3 (Ω)	92	112	122	132

3.4. The Influence of Z_3 on the Performance of the Proposed Filter

Table 3 shows the electrical parameters' values. Only the value of Z_3 is changed. The calculated scattering parameters of these four examples are illustrated in Figures 7(a) and (b). Obviously, the return loss performance in the passband of Example C_4 is the best among four examples, which is larger than 20 dB as shown in Figure 7(a). However, note that the number of reflection zeros of Example C_4 is six while the number of the other three examples is seven. What's more, the selectivity and operating bandwidth at 1 GHz changes slightly for all the Examples C_1–C_4, as illustrated in Figure 7(b).

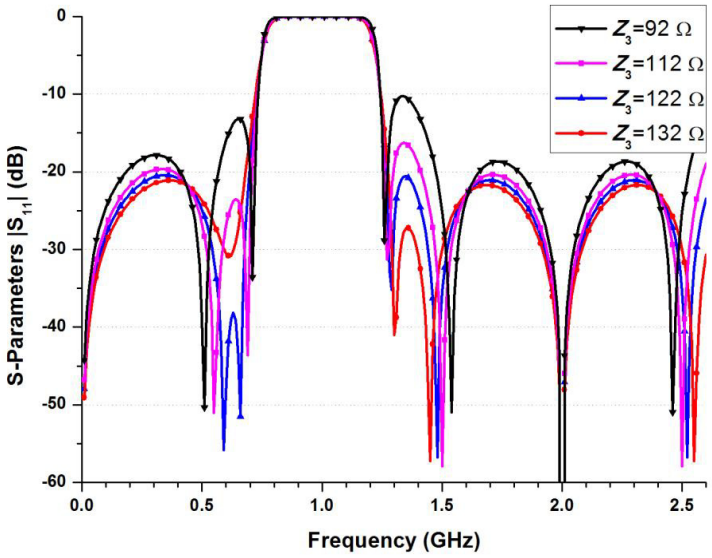

(a)

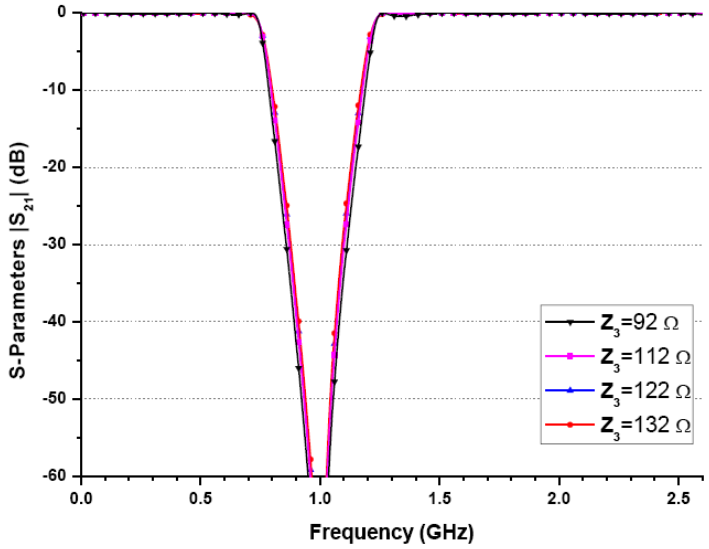

(b)

Figure 7. The scattering parameters (a) $|S_{11}|$ and (b) $|S_{21}|$ of the filter when $Z_3 = 92, 112, 122, 132\,\Omega$.

3.5. Design Examples of Ideal Filters

According to the number of transmission zeros, two types of ideal filters operating at 1 GHz are designed based on the previous analysis, especially Equations (11) and (12):

Case 1: This filter has only one transmission zero in the stopband with the following electrical parameters: $Z_T = 50\,\Omega$, $Z_{e1} = 140\,\Omega$, $Z_{o1} = 105\,\Omega$, $Z_{e2} = 140\,\Omega$, $Z_{o2} = 120\,\Omega$, $Z_3 = 122\,\Omega$, $\theta_{c1} = \frac{3}{4}\pi$, $\theta_{c2} = \frac{\pi}{4}$, $\theta_3 = \frac{\pi}{2}$. Based on the lossless transmission-line and coupled-line models, the calculated scattering parameters are shown in Figure 8. The 20-dB band-stop fractional bandwidth is about 29.44% (0.84 GHz–1.13 GHz) and the return loss in the passband is larger than 20 dB.

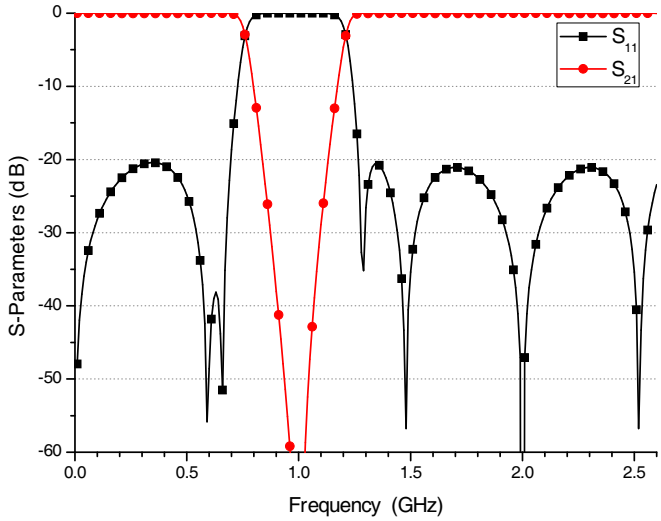

Figure 8. The calculated scattering parameters $|S_{11}|$ and $|S_{21}|$ of Case 1.

Case 2: Based on the analytical approach in Section 2 and Section 3, the filter with two transmission zeros in the stop-band can be obtained after tuning electrical parameters. Z_{e2} and Z_{o2} are modified as $Z_{e2} = 135\,\Omega$ and $Z_{o2} = 107\,\Omega$. The calculated scattering parameters are shown in Figure 9. The 20-dB band-stop fractional bandwidth is about 30.91% (0.83 GHz–1.14 GHz). However, the return loss in the passband is smaller than 20 dB.

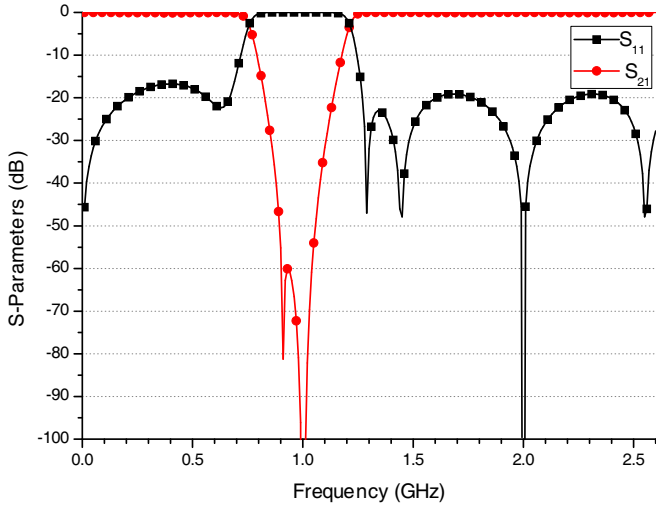

Figure 9. The calculated scattering parameters $|S_{11}|$ and $|S_{21}|$ of Case 2.

4. SIMULATED AND MEASURED EXAMPLES

To verify the design method, a standard filter is fabricated on Rogers R04350B with a relative dielectric constant of 3.48 and dielectric thickness of 0.762 mm. Figure 10 shows the microstrip layout (a) and the practical photograph (b) of the band-stop filter separately. The dimensions of this filter are determined as follows: $Ws = 1.8\,\text{mm}$, $W_1 = 0.25\,\text{mm}$, $W_2 = 0.2\,\text{mm}$, $W_3 = 0.25\,\text{mm}$, $L_1 = 70.8\,\text{mm}$, $L_2 = 22.9\,\text{mm}$, $L_3 = 47.3\,\text{mm}$, $L_S = 7.5\,\text{mm}$, $S_1 = 0.85\,\text{mm}$, $S_2 = 1.4\,\text{mm}$, $S_3 = 1.3\,\text{mm}$. A full-wave simulator Sonnet Lite has been applied to obtain and efficiently tune the physical dimensions. Measurements are carried out using an Agilent N5230C network analyzer. The simulated and measured scattering parameters and group delay performance are shown in Figure 11 and Figure 12 separately. As shown in Figure 11, the full-wave simulated and measured scattering parameters are in good agreement. The measured operating stopband of the filter is centered at 0.94 GHz (ideal value is 1 GHz) with a 3-dB cutoff frequency bandwidth of 58.2%. The attenuation levels in the band from 0.71 to 1.16 GHz are larger than 10 dB. The measured maximum attenuation level is −46.88 dB at 1.05 GHz (very close to the ideal value 1 GHz). The measured out-of-band return loss in the range of 0 to 0.65 GHz is larger than 10 dB while the measured out-of-band return loss in the range of 1.3 to 2.6 GHz is larger than

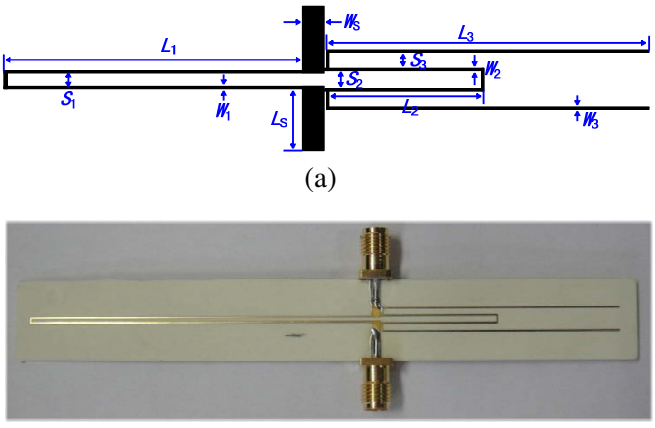

Figure 10. (a) The microstrip layout and (b) photograph of the band-stop filter.

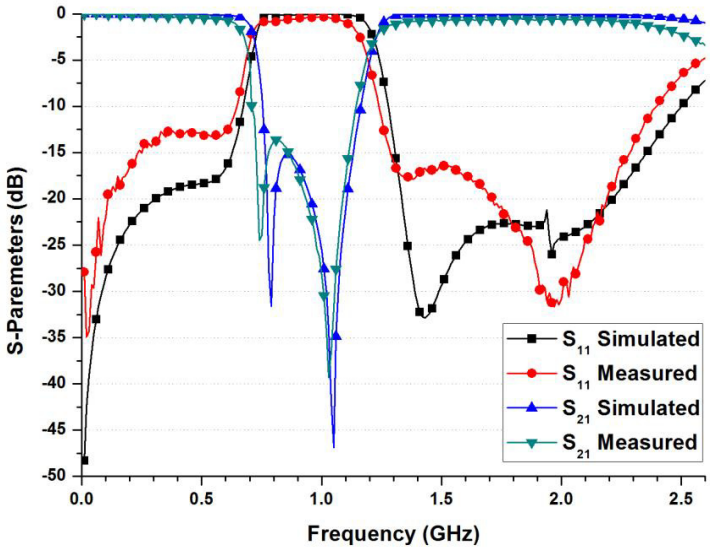

Figure 11. The simulated and measured results of the band-stop filter.

16 dB. The passband insertion loss is smaller than 1.57 dB in the range of 0 to 0.65 GHz and smaller than 1.15 dB in the range of 1.3 to 2.6 GHz. As shown in Figure 12(a), the maximum measured group delay is 2.43 ns while the minimum is 0.16 ns in the low passband (range from 0 to 0.65 GHz). As for the upper passband group delay shown in Figure 12(b), the maximum is 2.50 ns, and the minimum is 0.51 ns in the range of 1.23 to 2.6 GHz. Finally, in order to clearly highlighting the advantages of this proposed filter, the performance comparison with other recently published similar filters is listed in Table 4.

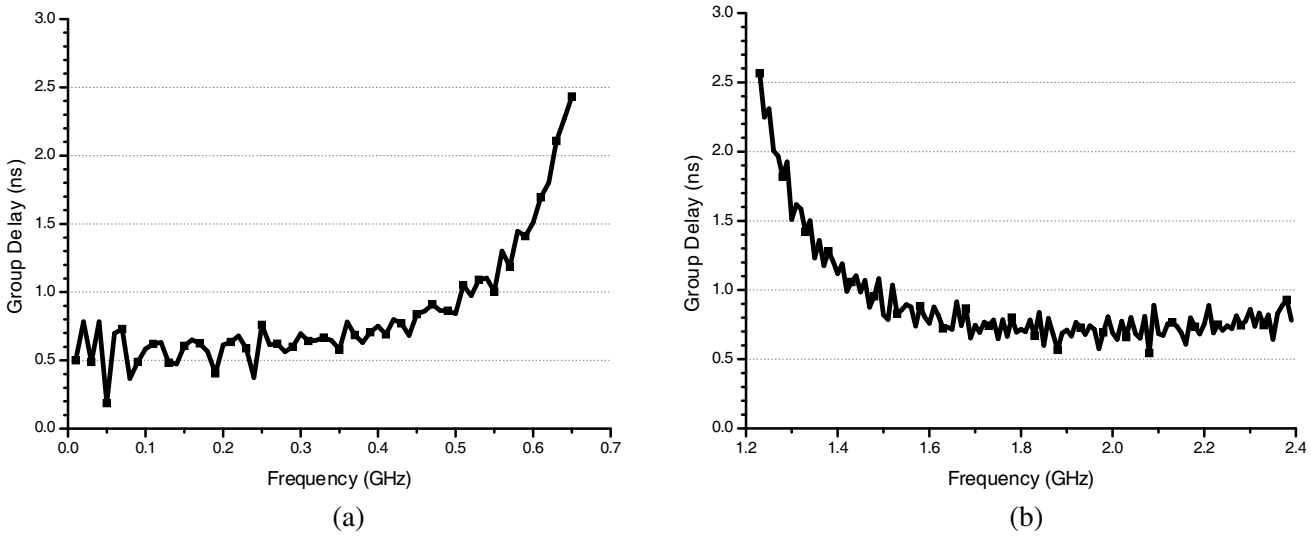

Figure 12. The measured group delay performance of (a) the low passband and (b) the upper passband of the band-stop filter.

Table 4. The comparison between the proposed and previous band-stop filters.

	Coupled-line implementations	Selectivity	Size	Bandwidth	Layout Feasibility
Ref. [2]	No	Low	Small	Narrow	High
Ref. [4]	No	High	Large	Wide	Low
Ref. [8]	Yes	Low	Large	Dual-band	Medium
Ref. [9]	Yes	Low	Medium	Wide	High
This work	Yes	High	Medium	Wide	High

5. CONCLUSION

A novel circuit configuration is proposed to construct a compact band-stop filter with large return loss, low insertion loss, sharp skirt selectivity, high attenuation level, and smooth group delay. The circuit configuration includes two parallel-coupled lines of different electrical lengths and open-circuit stubs. Five kinds of numerical examples have been demonstrated for comparison and two types of ideal filters have been designed. Then an ideal band-stop filter is chosen to fabricate on the practical substrate in microstrip, which proves that our proposed idea is correct and significant. This kind of coupled-line band-stop filter is expected to be widely used in microwave systems because it has a simple configuration and excellent performance.

ACKNOWLEDGMENT

This work was fully supported by "Training Programs of Innovation and Entrepreneurship for Undergraduates in BUPT (2014)" and in part by National Key Basic Research Program of China (973 Program) (No. 2014CB339900) and National Natural Science Foundation of China (No. 61201027).

REFERENCES

1. Hong, J.-S. and M. J. Lancaster, *Micro-strip Filters for RF/Microwave Applications*, Chapters 2 and 6, Wiley, New York, 2001.
2. Fallahzadeh, S. and M. Tayarani, "A compact microstrip bandstop filter," *Progress In Electromagnetics Research Letters*, Vol. 11, 167–172, 2009.
3. Wang, J., H. Ning, Q. Xiong, M. Li, and L. Mao, "A novel miniaturized dual-band bandstop filter using dual-plane defected structures," *Progress In Electromagnetics Research*, Vol. 134, 397–417, 2013.
4. Velidi, V. K., A. B. Guntupalli, and S. Sanyal, "Sharp-rejection ultra-wide bandstop filters," *IEEE Microwave and Wireless Components Letters*, Vol. 19, No. 8, 503–505, 2009.
5. Wu, Y. and Y. Liu, "A coupled-line band-stop filter with three-section transmission-line stubs and wide upper pass-band performance," *Progress In Electromagnetics Research*, Vol. 119, 407–421, 2011.
6. Wu, Y., Y. Liu, S. Li, and C. Yu, "A simple microstrip bandpass filter with analytical design theory and sharp skirt selectivity," *Journal of Electromagnetic Waves and Applications*, Vol. 25, Nos. 8–9, 1253–1263, 2011.
7. Mrinal, K., K. Vamsi, S. Sanyal, and A. Bhattacharya, "Design of ultra-wideband band-stop filter with three transmission zeros," *Microwave and Optical Technology Letters*, Vol. 50, No. 11, 2955–2957, 2008.
8. Wang, W., M. Liao, Y. Wu, and Y. Liu, "Small-size high-selectivity bandstop filter with coupled-line stubs for dual-band applications," *Electronics Letters*, Vol. 50, No. 4, 286–288, 2014.
9. Cui, D., Y. Liu, Y. Wu, S. Li, and C. Yu, "A compact bandstop filter based on two meandered parallel-coupled lines," *Progress In Electromagnetics Research*, Vol. 121, 271–279, 2011.